Forming and Maintaining a Potential Well in a Quasispherical Magnetic Trap

by Nicholas A. Krall, Krall Associates, Del Mar, CA 92014, <nkrall@aol.com>

Michael Coleman, Kenneth C. Maffei, John A. Lovberg, and R. A. Jacobsen, Directed Technologies, 3601 Wilson Boulevard, Suite 650, Arlington, VA 22201, <info@directedtechnologies.com>

Robert W. Bussard, Energy/Matter Conversion Corporation, 680 Garcia Street, Santa Fe, NM 87505, (505) 988-8948, <emc2qed@comcast.net>

Abstract

The formation and maintenance of an electrostatic potential well by injecting electrons into a quasi spherical cusped magnetic confinement geometry is studied experimentally, as a function of plasma fill density and of the energy and current of the injected electrons. A model is developed to analyze the experiment. It is found that the potential is comparable to the energy of the injected electrons at low density, and decreases as an increasing density of cold plasma fills the device because of ionization or wall bombardment. Implications for fusion based on electrostatic/magnetic confinement are discussed.

I. Introduction

Present-day fusion research is based on two approaches. Magnetic fusion confines a hot dense Maxwellian plasma magnetically, with only the more energetic parts of the ion velocity distribution participating in the fusion process. Inertial confinement fusion deposits a large amount of energy (in the form of laser light or ion beams) on the surface of a small solid target, causing an imploding compression wave that raises the density enough to trigger a fusion reaction. However, a third possibility has long been suggested,[1,2] though not much studied, namely, fusion produced by a cloud of converging ions, dense only near the center of a sphere, confined by electrostatic potentials produced by grids, and having a velocity distribution far from thermal equilibrium, being instead peaked near the energy at which the fusion cross sections are maximum.

An approach to fusion has been proposed by Bussard,[3,4] which keeps the advantages of convergent ions and electrostatic confinement without the disadvantages of wires imbedded in the plasma. The idea is that in a plasma with a slight excess of electrons, a quasi-spherical cusped magnetic field, Figure 1, would confine the electrons, while the electrostatic potential from the electron excess would confine the ions, and accelerate them to a dense focus at the center, where the probability of fusion would be high.[4,5] The magnetic field can be formed by a set of high-order polyhedral windings that produce a quasi-spherical array of point cusps,[6] in a magnetic geometry called a Polywell. The physics of this idea has been discussed in detail elsewhere,[4,5] but clearly a central feature is the need to form and maintain an excess of electrons sufficient to provide a substantial electrostatic potential. Injection from high-energy electron guns seems the only practical way to achieve this.

Recently an experiment was constructed to test some elements of this approach to fusion. The research activities included detailed studies on the injection and trapping of high-energy electrons in a Polywell magnetic field, both with and without a background plasma. By varying the parameters of the electron guns and the background plasma, information was obtained on many properties of the system, including plasma confinement, recycling of plasma from the walls, and breakdown of a neutral fill gas. Most important, however, was the information about the properties of the potential well formed by electron injection, including its depth, radial profile, time history, and dependence on system parameters.

In this paper we describe these measurements, along with theoretical models, which help understand them.

In Section II we briefly describe only the aspects of the experiment and diagnostics relevant to the present paper. In Section III we describe the formation of a potential well when electrons are injected into vacuum. In Section IV we describe and analyze experiments in which electrons were injected into a background prefill gas, and the potential measured, for various. values of fill density and electron gun properties. In Section V we discuss the results, as well as the implications of these experiments for the Polywell fusion scheme. In the Appendix we describe the formation and decay of a cool dense plasma in the Polywell produced by radio frequency (RF) ionization of a prefill neutral gas; this study is directly relevant to the work discussed in Section IV, because it develops and benchmarks a model that reproduces experimental results on breakdown and confinement. This model can then be used with some confidence in the electron injection experiment.

II. The HEPS Experiment

The High-Energy Power Source (HEPS) experiment constructed at Directed Technologies Incorporated (DTI) used a motor generator set designed to provide in excess of 4000 Amp at 4 kV to six series-connected field coils in approximately 225 ms, with 8 MJ of stored energy, to produce the Polywell magnetic field[6] shown in cross section in Figure 1. This magnetic field has the same structure whether viewed in the x-y, y-z, or x-z plane, with the plane passing through x=y=z=0.

Electrons were injected into three of the magnetic cusp throats, from electron guns capable of operating in the range 5-10 kV and 5-15 Amp. In these guns, electrons were emitted from a cathode, accelerated through an anode structure and allowed to pass through a drift tube region into the tank. Particle simulations and particle-in-cell (PIC) codes[7] showed that electrons must be injected along field cusp lines in order to access the central volume of the magnetic well.

The electron beam power supplies could produce 20 Amp at 20 kV for a maximum 25 ms pulse with a minimum current droop (<10%) for each of three electron guns. The pulse width and charging voltage were variable, the rise time for the system was less than 30 μs, and the size of the extracted electron beam was 2 cm in diameter.

The parameters of the experiment are given in Table 1. In some experiments the electrons were injected into a vacuum; in others the device was prefilled with a neutral gas or a plasma. In the prefill case, the neutral gas background was introduced using a system of piezoelectric puff valves prior to electron injection. A 10 kW, 2.45 GHz RF source was then used to break down the neutral gas background.

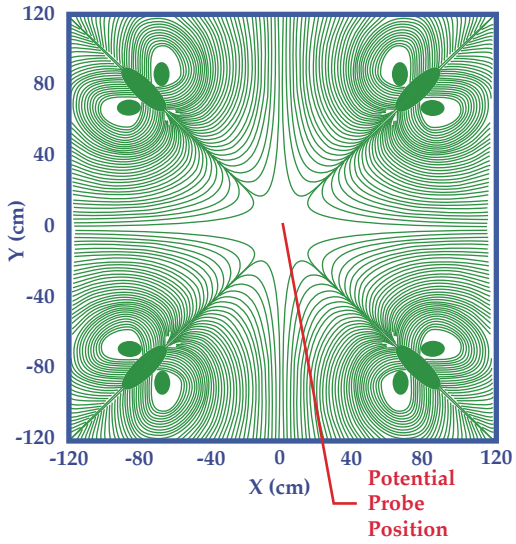

Figure 1 — Equatorial flux lines

The diagnostics relevant to the present paper included a probe or set of probes inserted into the plasma to measure the potential relative to the wall. This diagnostic consisted of a capacitive-divider potential probe[8] which sampled the potential at 54 radial positions. In the standard operating regime, the confining field was 1.5 kG at the major point cusps, and the probe was inserted at the midplane 10° off the cusp axis (Figure 1). The probe measured true space potential to within $0.5T_e$.

Table 1 — Experimental Parameters

Plasma region	80 cm radius sphere
Magnetic field	B_0r^3/R^3, B_o=1.5 kG
Pulse time	B = constant for 10 ms
Electron gun	20 Amp at 20 kV each
Power supplies (3)	I/E = constant

A second diagnostic was a 94 GHz microwave interferometer. This system is of the Mach-Zender design, in which the probe beam is split, undergoes one pass through the plasma, and is recombined on the other side of the tank. Four chords were employed at 0, 6, 13, and 28 cm from the tank center. With a path length of ~2 m, the system resolution was ~5 x 10^9 cm^{-3}.

A third diagnostic was a Langmuir probe (diameter 2 mm), used to estimate the electron density. This diagnostic was used because in many of the experiments, the plasma density was below the resolution of the interferometer. The probe was mounted on a flexible bellows, which made it possible to place the probe tip at any radius in the chamber; it was inserted at the midplane 10°

off the cusp axis, as was the potential probe described above. An adjustable bias (-100 to + 100 V) was applied to the probe tip, and the current drawn by the probe was measured as a voltage drop across an 18 Ω resistor connected to ground.

Initial tests with the Langmuir probe were performed with an electron cyclotron resonance (ECR) produced plasma to verify its correct operation. The probe bias was varied on each ECR shot to obtain a typical Langmuir probe *I-V* characteristic (T_e = 12-15 eV) for the ECR plasma. The electron saturation current was used to determine the plasma density; the calibration of the Langmuir probe was obtained by measuring the plasma density with the microwave interferometer and the electron saturation current on the same shot. The calibration obtained was consistent (within 50%) with that expected using simple Langmuir probe theory (neglecting *B* fields).

In some data runs, we utilized the probe to determine the plasma density existing in the vessel prior to the firing of the e guns, especially in the cases where the density was below the resolution of the interferometer. Once the e guns are fired, the high-energy, non-Maxwellian electrons prevent a simple interpretation of the signals obtained to infer density or the temperature. However, the probe signal can still be used in a semi-quantitative fashion by subtracting the high-energy electron current flux to the probe, determined from the observed electron gun current, to estimate the saturation electron current from the background plasma.

Finally, an energy analyzer was used to obtain at least grossly, the energy distribution of the higher-energy electrons in the system. This diagnostic, placed at a cusp at the bottom of the vacuum vessel, included a pair of grounded grids, an electron repeller grid that can be biased from 0 to -15 kV, an ion repeller grid that can be biased from 0 to + 15 kV, a secondary electron grid that is biased at -30 V, and a collector plate.

The intent of the experiments described here was first to demonstrate that an electrostatic potential well could be formed and maintained, both in a vacuum and in a system with background plasma, and second to see if the characteristics of the potential in various ranges of gun energy and current and various pre-fill densities were understandable on the basis of straightforward classical models. In other words, we asked whether there were any obvious anomalies in this portion of the Polywell fusion scenario. The results described in the next section, along with the experiments described in the Appendix, lead us to conclude that potential well formation in the Polywell follows a predictable and understandable path.

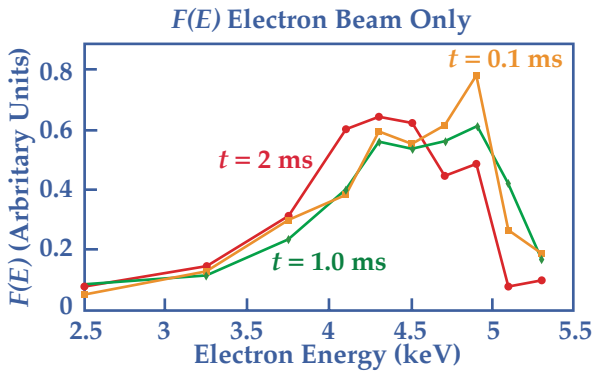

Figure 2 — Electron beam thermalization (e-guns at 5 kV)

III. Electron Trapping and Potential Well Formation-Electrons Only

One issue involving the cusp confinement aspect of the HEPS experiment is whether electrons injected into a point cusp will be confined at all; will injected electrons simply find their way out of a point cusp on an opposite face in a single transit.[7] This should not be a problem, since on passing through the center of the device, where *B* = 0, the electrons lose the invariance of their magnetic moment and other adiabatic constants.[9] Nevertheless, it was important to demonstrate trapping. The aim of this section is to show that the electrons are, in fact, trapped, and that their confinement time is consistent with theoretical expectations.

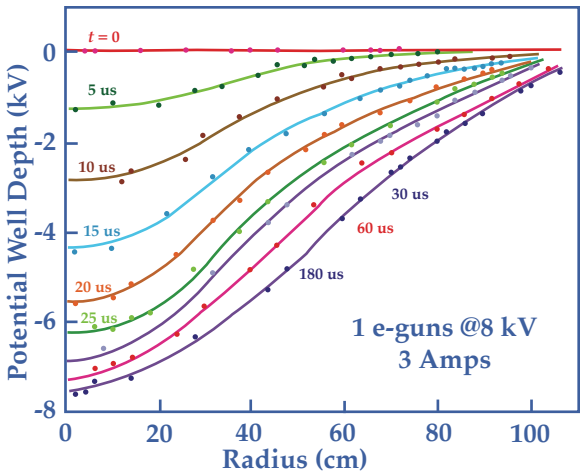

Figure 3 — Potential profile, electrons only — one electron gun

The strongest evidence that trapping automatically occurred came from the measured buildup of the potential well to approximately the gun voltage, a value that is inconsistent with the potential that would result from the space charge of transiting electrons. A second bit of evidence was the observation that the energy distribution of electrons leaving the device changed (broadened) with time (Figure 2), at a rate of $d(\Delta E)/dt \sim$ 500 eV/ms;

this indicates an electron dwell time much longer than the 10^{-7} s transit time of a 5 keV electron.

To quantify the argument that the potential observed shows electron trapping, consider a current I = 5 Amp from an electron source of energy E = 5 kV injecting electrons into a confinement region of volume πR^3 and diameter $2R$. The transit time of electrons is:

$$transit\,time \equiv t_T \sim \frac{2R}{\sqrt{2E/m_e s}} \quad (1)$$

and the density of a plasma of unconfined electrons would be:

$$n_e \sim \frac{It_T}{e\pi R^3} \quad (2)$$

from $\nabla^2\phi = 4\pi e n_e$, a potential of order:

$$(e\phi)_{noconfinement} = 600\left(\frac{I}{5A}\right)\sqrt{\frac{5kV}{E}} \quad (3)$$

would develop due to these unconfined electrons.

Figure 3 shows the potentials measured at various radii as a function of time by the probe described in Section II. The well forms in about 60 μs, which is also the time buildup of the cathode potential (= the electron energy) from the gun. For the one-gun case in Figure 3, 3 would give:

$$(e\phi)_{noconfinement} \sim 0.3kV \quad (4)$$

while the experiment shows:

$$(e\phi)_{actual} \sim 8kV \quad (5)$$

Similar results are obtained with three e-guns. This shows that the electrons are trapped in the cusp field, i.e., are not lost in a single transit, so that the electron density is determined by electron (or plasma) confinement in a cusp, which we address in the remainder of this section.

The potential can be used to infer the electron density, which gives an indication of the confinement time; the density was too low to be detected directly by the interferometer. Using Poisson's equation and assuming spherical symmetry, we compute the electron density profiles from the potential profiles with the result shown in Figure 4. At 10 μs, with an average current of 1 A (total from three guns at this phase of the initial current rise) entering the chamber, the total measured stored electron inventory of 8 x 10^{11} implies an effective electron confinement time of about 130 ns if all the gun electrons entered the chamber. However, since $e\phi \simeq E_{gun}$, a virtual cathode will form that will reject much of the gun current. Measurements of cusp losses account for less than 10% of the gun cathode current, implying that a large amount of the gun current is lost in the gun drift tube before entering the chamber. If the current exiting the gun throat is, in fact, being 90% choked by the presence of the virtual cathode in the chamber, then the measurements imply an electron confinement time of about 1-2 μs.

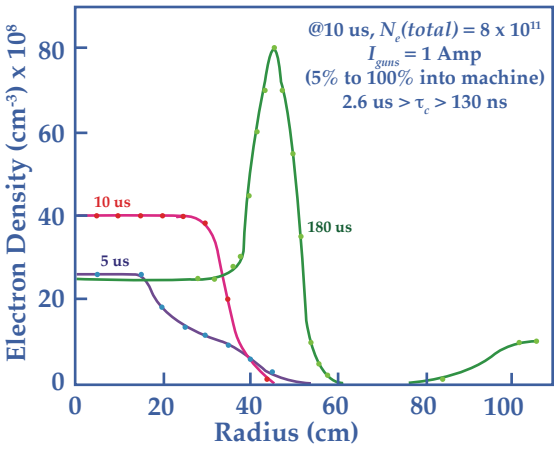

Figure 4 — Electron density profile calculation

The theoretical estimate[10] of hot electron confinement in a mirror model (low β) Polywell is in the range 0.5-2.5 μs, which overlaps the experimentally inferred range. This estimate is produced by the following argument: assume that at low density the cusp acts as a magnetic mirror in confining plasma. The mirror ratio is B_{max}/B_{min}, where B_{max} is the field in the cusp throat and B_{min} is the field at the interior point where B has gotten just large enough so that the electrons are adiabatic. The effective collision frequency that fills the mirror loss cone is $\tau_c = 2R/v$, the transit time across the device. This is because in each transit through the low B interior the electrons lose their adiabatic invariance, as if they have had a collision. This argument gives:

$$\tau_{confinement,\,mirror\,\mathrm{mode}} \simeq \frac{2R}{v}\left(\frac{B_{\max}}{B_{\min}}\right) \quad (6)$$

where v is an average electron velocity during the transit. We explicitly note that:

$$\left(\frac{1}{B}\frac{dB}{dr}\right)_{r_a} \equiv \frac{3}{r_a} = \frac{1}{a_L} \equiv \frac{e}{vmc}\frac{B_0 r_a^3}{R^3} \quad (7)$$

where we have taken $B = B_0 r^3/R^3$, determines the radius r_a at which the electrons become adiabatic. Then $B_{min} = B_0 r_a^3/R^3$ determines the mirror ratio and the confinement time in the low-density regime of the experiment. Equation (6) is unchanged by the presence of a background plasma, since the effective collision frequency of electrons (= $1/t_T$) is many orders of magnitude greater than that of Coulomb collisions, even in a dense plasma.

The reason that 6 implies a range (0.5-2.5 μs) of confinement rather than a single confinement time is that the average transit time R/v depends on both the electron energy and the depth and shape of the potential well, which can only be bracketed.

IV. Electron Trapping and Potential Well Formation, Dense Background Plasma

In Section III we showed that electrons injected through a cusp throat into a vacuum were trapped and formed a potential comparable to the gun potential; in this section we describe a set of experiments in which the injection was done into an increasingly dense plasma, formed by prepuffing a neutral gas, partially ionized by RF which was resonant with electron gyrofrequencies inside the chamber, prior to firing the electron guns. Figure 5 shows the time history of the central potential for increasing levels of plasma prefill density, on a short and long time scale. The most obvious feature is that the potential forms when the guns are fired, and drops sharply at 3 ms, which is the gun pulse length, t_{gun} = 3 ms.

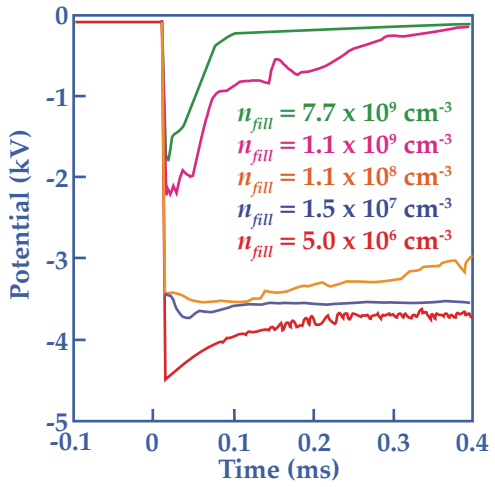

Figure 5a — The dependence of the plasma potential on the initial background plasma density, on a short time scale

On a time scale comparable to the 30 μs rise time of the gun, the rise of the potential is similar in size and profile to the case of injection into a vacuum (compare Figure 3 and Figure 6). When the prefill is of very low density, the potential persists until the gun turns off. However, as the prefill density is increased, the potential quickly falls below its peak value to an increasingly small level. These trends are shown in Figure 5a.

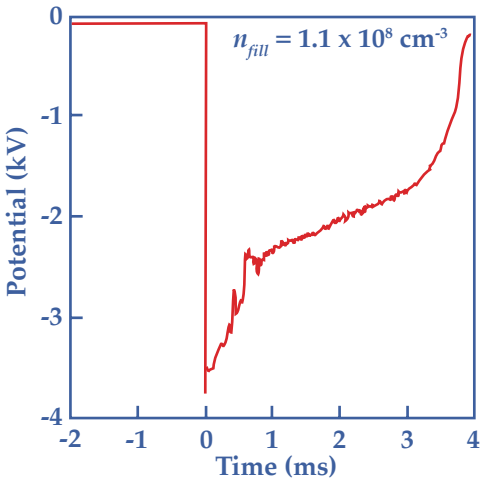

Figure 5b —The dependence of the plasma potential on the initial background plasma density, on a long time scale

Because the failure of the potential to persist when the density of the neutral background far exceeds the unneutralized density that forms the potential (which will also be the conditions on a reactor scenario[1,4]) might be interpreted as a flaw in the concept, it was important to understand this behavior. To this end we carried out a set of studies to understand the behavior of the background plasma itself (given in the Appendix), and then a set of studies to understand the behavior of the potential as a function of background density, electron energy, and electron current (described below).

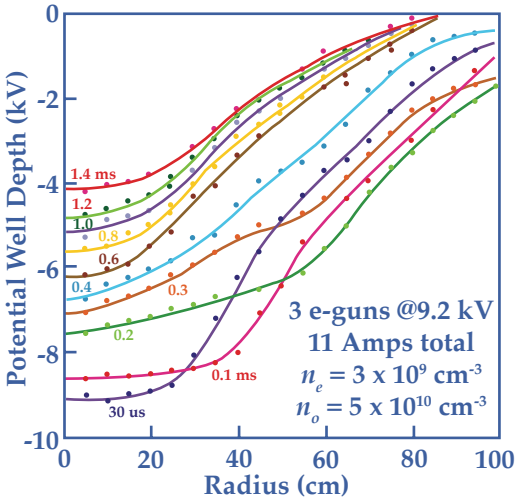

Figure 6 — Potential well behavior 10° off a cusp line during plasma density buildup (no RF).

We conclude, following these studies, that the behavior of the potential is a predictable property of the interaction of the very weak current of hot electrons with the much denser current of the cold electrons of the background gas, and has no unexpected implication for a reactor scenario, where virtually all the electrons would originate at high energy, from the high voltage guns.

A. Experimental data relating to maintenance of the potential

1. Potential versus prefill plasma density

The standard experimental conditions were that an electron current of 4 Amp was injected into the HEPS cusp field with energy 5 kV. Figure 5a shows the behavior of the central potential for various values of plasma prefill, with the electron guns being fired at 2.01 ms. Figure 5b shows the same parameters on a longer time scale, for a single value of prefill density. The trend is that the potential rapidly rises to a peak value that is higher for lower values of prefill density. This peak potential drops on a time scale of <0.1 ms to a more slowly varying potential, which is also higher for lower values of prefill density.

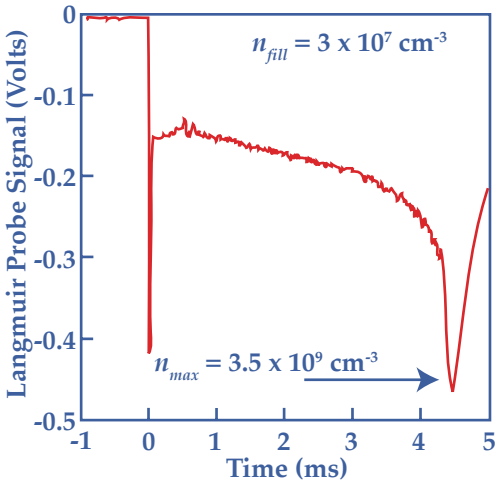

Figure 7a — The time history of plasma density, for n_{fill} = 3 x 10^{7} cm^{-3}

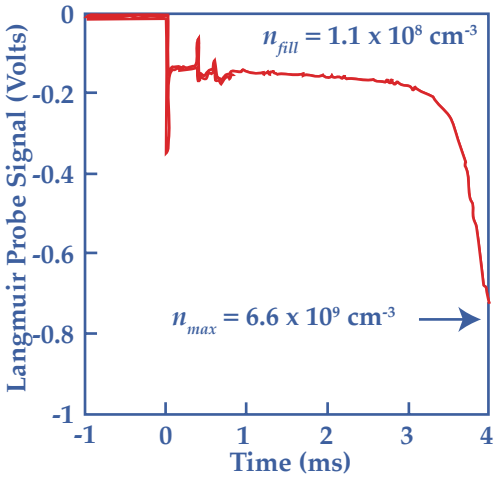

Figure 7b — The time history of plasma density, for n_{fill} = 1.1 x 10^{8} cm^{-3}

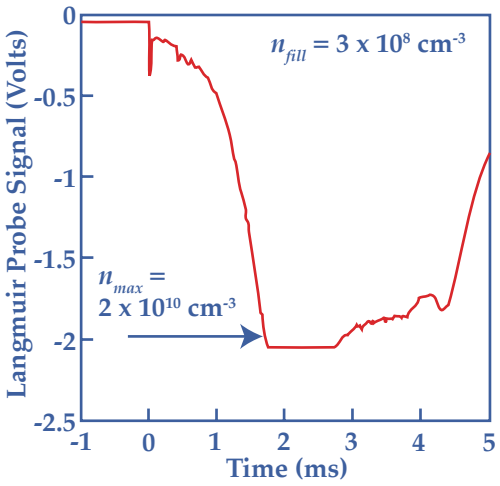

Figure 7c — The time history of plasma density, for n_{fill} = 3 x 10^{8} cm^{-3}

2. Electron density versus time

There are at least two effects which can lead to a time variation of the potential produced by the excess electrons in the device. One is a transient effect of the plasma, in which it changes its density profile as well as its energy distribution (see Figure 11), while evolving toward a quasi-steady state after the turn on of the electron guns.

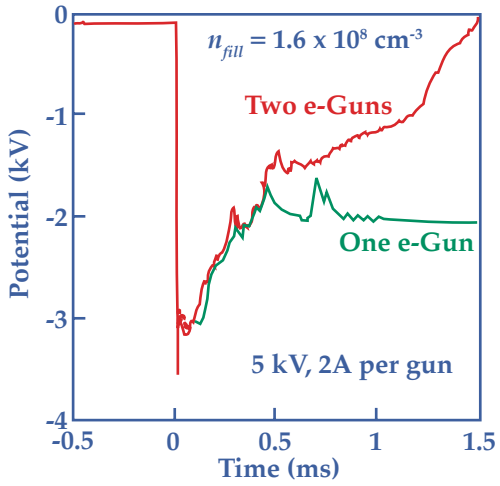

Figure 8a — The dependence of the potential on the hot electron current

A second is the change in the magnitude of the background plasma density due to the production or loss of plasma or hot electrons in the device. To help separate these effects, Figures 7a-7c show the current to a Langmuir probe that measures the electron density, for three different values of plasma fill density, with the e-guns fired at 2 ms. The density rises to a value of about 100 times greater than the fill density (see Section IV.B.2 for an explanation of this fact), over a time of order 2 ms for

the higher prefill example, and over a time of order 4 ms in the lower (by 10x) prefill example.

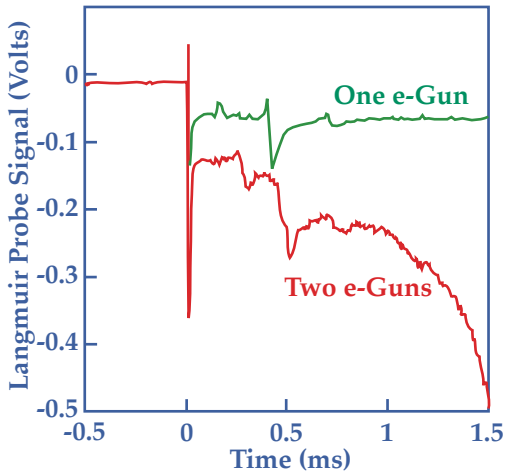

Figure 8b — The dependence of density on the hot electron current

3. Potential versus Injected Electron Parameters

To study the change in potential and density with changing electron parameters, Figures 8a and 8b show the time variation of the potential and of the signal on a Langmuir probe, which we believe to be proportional to the plasma density (after subtracting the signal due to fast electrons). In the case shown, the injected electron current was reduced from 4 Amps in one run to 2 Amps in the next, by turning off one of the electron guns.

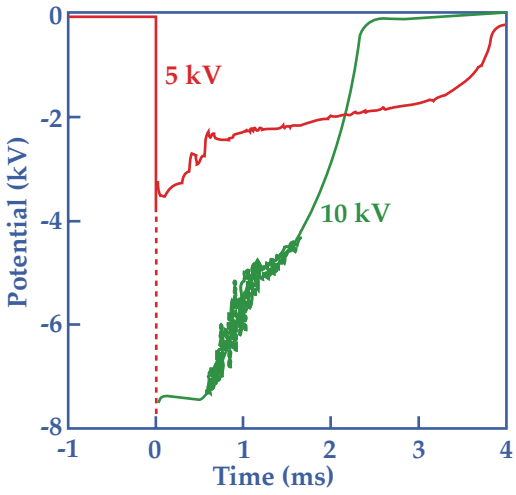

Figure 9a— The dependence of the potential on the hot electron energy

The trend is that a transient of about 0.5 ms, during which the potentials in the two cases are roughly comparable, is followed by a period in which the larger current produces a potential that is lower than that produced in the smaller current case, and continuing to decrease with time. In this case, at least, more does not prove to be better in terms of producing a potential.

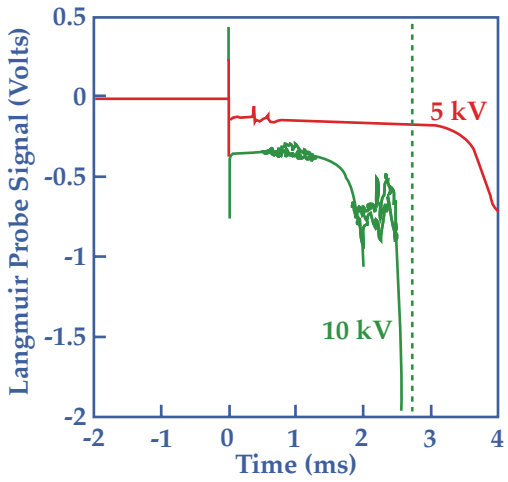

Figure 9b— The dependence of the density on the hot electron energy

In Figures 9a and 9b, the potential and density are measured in a case where the energy of the injected electrons is increased from 5 kV in one run to 10 kV in the next. The 10 kV case also injects 10 Amps of current, compared with 4 Amps in the 5 kV case, because of the characteristics of the electron guns. The trend is that the high-energy, high-current case initially produces a deeper potential well than does the lower-energy, lower-current case. However, at later time, after ~2.5 ms, the higher-current higher-energy case has a much weaker potential than the other case. Correspondingly, the density in the high-current case increases dramatically at ~2.5 ms after the guns are fired, as is clear from Figure 9b.

4. Radial Variation of the Potential

Further information can be obtained from measuring the radial dependence of the potential. This data is shown in Figures 10a and 10b, for two different values of prefill density. In this case, the trend is that the potential in the lower density case varies fairly smoothly with radius, in contrast with the higher-density case, in which the potential seems to be substantially flatter in the center, with the electric field it produces being more localized toward the edge. This statement is only true before the complete collapse of the potential that as is the case with the density peak, takes place much earlier in the high prefill case than in the low prefill case.

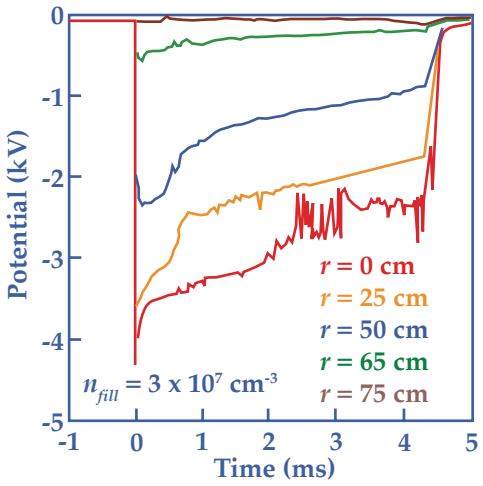

Figure 10a — Radial profile of the potential for a low prefill density

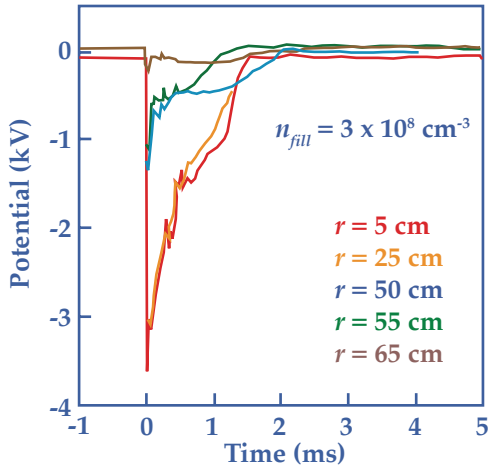

Figure 10b — Radial profile of the potential for a high prefiil density

5. Energy distribution

To estimate the energy of trapped electrons, as a function of time, we examine electrons escaping through the face cusp. Their energy distribution was found by first measuring the loss current for a number of electron repeller biases (in the range 0-5.5 kV) and fitting the resulting data with a third degree polynomial. This polynomial was differentiated to obtain the electron distribution, with the result shown in Figure 11.

The trend here is that at 0.1 ms after the guns are fired to inject a mono-energetic current of electrons at 5 kV, the electrons are observed to have an energy spread of several kV, peaked at 4 kV, while at later times the mean energy decreases, with the distribution peaked at lower energies, below 0.5 kV.

B. Interpretation of the observations

In this section, a model is developed for the interaction of a hot unneutralized electron swarm with a plasma background, including a description of the influence of the background on the potential produced by the unneutralized hot electrons, as well as a model for the formation and decay of the prefill plasma by ionization of a background gas of neutral atoms by a radio frequency wave source, and subsequent decay after the RF was turned off. Some elements of the model are supported by the experiments described in the Appendix.

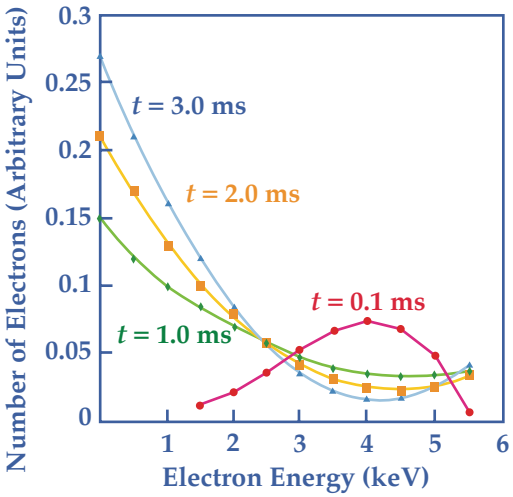

Figure 11 — Time history of the electron energy distribution

1. Potential versus prefill plasma density

Energy conservation will connect the potential produced by an electron cloud with the density of a background plasma. Because the background electrons tend to acquire an energy comparable to the depth of the potential well, and because the total kinetic energy of the system cannot exceed the energy of the injected electrons, there is a bound to the potential, given by:

$$\int d^3 r n_h e\phi_{gun} \geq \int d^3 r n_b e\phi$$

$$\simeq \int d^3 r f_b(r,v)\left(\frac{1}{2}mv^2\right)d^3 v \qquad (8)$$

where n_h is the density of the hot injected electrons, n_b is the density of the cooler background plasma produced by ionization of the background gas, and f_b is the velocity distribution of the background plasma, emphasizing that the mean energy of the background plasma must be comparable to the actual plasma potential. Further, the shape of the potential is given by a self-consistent solution to Poisson's equation:

$$\frac{1}{r^2}\frac{\partial}{\partial r}r^2\frac{\partial\phi}{\partial r} = 4\pi e n_h + 4\pi e n_{be}\exp\left(\frac{e\phi}{T_e}\right) - 4\pi e n_{bi}\exp\left(-\frac{e\phi}{T_i}\right) \quad (9)$$

where the n_b's are the densities the plasma produced by ionizing the background gas would have if there was no potential well, i.e., if ϕ=0, whereupon $n_{be} = n_{bi} = n_b$. Equation 9 can be solved if we assume that the background temperature is larger than the potential, leading at once to:

$$\phi_{\max} = \frac{1}{3}\frac{n_h}{n_b}\left(\frac{4\pi}{3}en_hR^2\right) \quad (10)$$

This overestimates the influence of the background density on the potential, because, in fact, $T \le e\phi_{max}$. Assuming that $T << e\phi_{max}$ would give $e\phi \sim \ln n_b$.

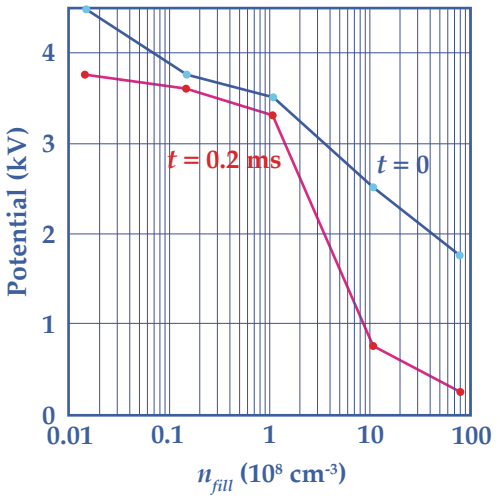

Figure 12 — Potential versus density at early and late time

Comparing with Figure 5 confirms the trend that higher plasma density gives lower plasma potential, for the same density of unneutralized hot electrons. In a more quantitative manner, Figure 12 plots the potential deduced from Figure 5 as a function of background plasma density. The behavior is clearly much weaker than $1/n_b$.

The fact that the potential consistently decreases with time is also consistent with the model, if the background density increases with time. Theory and experiment for the time behavior of background density with time are discussed below.

2. Electron density versus time and prefill density

The results described above show clearly that the plasma density controls the potential produced by a given electron gun current. Therefore it is important to understand the physics that control the electron density.

In the Appendix, we demonstrate that the time behavior of the plasma density produced by ionizing a prefill gas using a bath of radio frequency waves can be understood by a model which includes the interaction of the plasma with the wall of the experimental device. The wall provides a source of neutrals whose density depends on the escape rate of plasma from the device, and that can be ionized by collisions with the ambient electrons. The fact that the peak density of electrons in the device is observed to be much greater than the fill density, as shown in Figure 7, is therefore not surprising.

Table 2 — Plasma Density at 4.5 ms after the Guns are Fired

n_0 (cm^{-3})	$n_{p,\,theory}$ (cm^{-3})	$n_{p,\,exp}$ (cm^{-3})
3 x 10^7	3.8 x 10^9	3.4 x 10^9
1.1 x 10^8	6 x 10^9	7 x 10^9
3 x 10^8	1 x 10^{10}	1.8 x 10^{10}

The density reached by the plasma when the electron guns are on is a strong function of the prefill plasma density. To understand this, we use the model formulated in the Appendix, including the effect of the hot electron component, which both helps ionize the background neutrals, and by colliding with the wall increases the inward flux of neutrals. Taking the hot electron density to be constant (the gun replenishes the losses), and using the same neutral background density and ionization cross sections as in the Appendix, we write:

$$\frac{dn_e}{dt} = -\frac{n_e}{\tau_e} + n_e n_0 \sigma_1 v + n_{eH} n_0 \sigma_2 v \quad (11)$$

$$\frac{dn_0}{dt} = -n_e n_0 \sigma_1 v - n_{eH} n_0 \sigma_2 v + \frac{e}{\tau_e} + \frac{eH}{\tau_{eH}} \quad (12)$$

Equation 12 assumes that each electron striking the wall produces one wall neutral. In the Appendix, a study of the density produced by RF ionization of a prefill gas establishes that after a transient in which relatively weakly bound surface material is bombarded from the wall, a one-to-one ratio of electrons striking the wall and neutrals coming off it is needed to explain the fact that the electron density is observed to reach a steady-state value. Taking specific values for the various parameters, τ_e = 0.5 ms, $\sigma_1 v$ = 3.33 x 10^{-8} cm^3/s, n_{eH} = 5 x 10^8 cm^{-3}, $\sigma_2 v$

= 0.1 x 10^{-8} cm^3/s ($\sigma_2 v < \sigma_1 v$ because the energy of the hot electrons is so large compared with the ionization threshold energy of H_2),[11] $\tau_H = 5 \times 10^{-5}$ s, we can integrate Equations 11-12 numerically, for several values of plasma prefill. Table 2 gives the density at 4.5 ms after the electron guns are fired, both from the experiment and from the theory. Figures 13 and 14 give the time variation of density for two values of prefill. The results are in reasonable agreement with experiment.

Clearly, better agreement could be obtained by adding more physics to the model. For example, higher density would give lower background plasma energy, and therefore longer confinement times. This would have the effect of increasing the electron production rate, which would be in the direction of making theory and experiment in Figure 13 come into closer agreement. Also, changing the initial values of hot electron density, neutral gas density, and hot electron ionization cross section would allow fine tuning of the results. However, the fact that even the simplest model that contains the essential physics gives qualitative agreement between theory and experiment encourages us to believe that we understand the physics behind the experimental results on density versus time, both as to the timing of the rapid rise and as to the actual density increase.

Last, the results in this section coupled to the discussion in Section IV.B.1, which connects the decrease of plasma potential with an increasing background plasma density make the later time behavior shown in Figure 5 reasonable, namely that the density increases and the potential crashes.

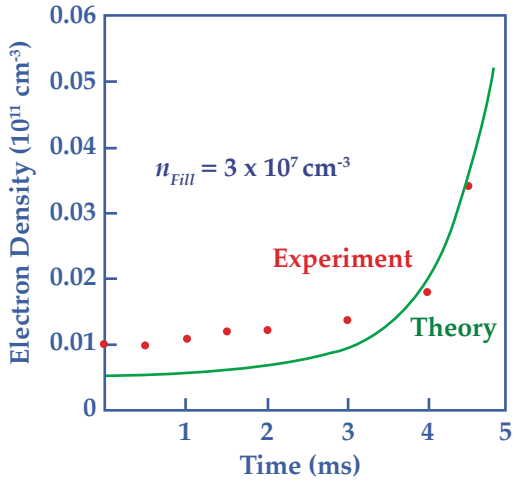

Figure 13 — Calculated plasma density for plasma pre-fill = 3 x 10^7 cm^{-3}

3. Potential versus injected electron parameters

When the current from the electron guns is increased, the initial potential should not be expected to change, since when the potential reaches the value of the gun energy, the virtual cathode formed by the already injected electrons shuts off the gun current, maintaining $e\phi_{max} = E_{gun}$. Figure 8b shows that at 2.5 ms, the density in the two-gun run begins to rapidly increase, greatly exceeding the density in the one-gun run. The fact that before 2.5 ms the probe signal indicates a difference in density without a difference in potential is not particularly surprising, since the radial profile of the potential can be somewhat different in the two cases, where the density is still primarily hot electrons. The drastic change when $n_{\sim b} >> n_{\sim hot\ electron}$ is a much stronger indicator of the effect of the background.

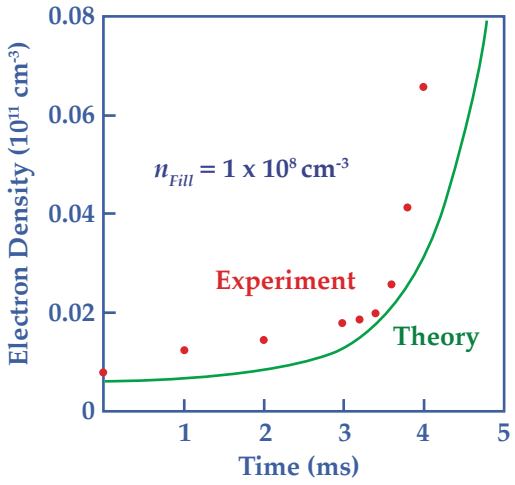

Figure 14 — Calculated plasma density for plasma prefill = 1.1 x 10^8 cm^{-3}

The runs shown in Figure 9 are complicated by the fact that both the energy of the injected electrons and the current change. Nonetheless, the results are still easy to understand on the basis of the models described above. First, the initial potential follows. the gun energy, as expected. Second, at about 3.5 ms, the higher current run produces a much denser background plasma, as suggested by Equations 11-12. At the same time, the potential produced by the higher-energy electron gun drops below that of the lower-energy case. Based on the analysis discussed in Section IV.B.2, the higher current produces a higher background density than does the lower current, and it does it faster. Thus, since we have also determined that higher-density produces lower potential, the drop of the potential in the 10 kV gun case relative to the 5 kV gun case is expected.

4. Radial variation of the potential

With no background plasma, the potential builds up to the gun energy; this potential prevents further buildup of unneutralized electrons, thus clamping the unneutralized electron density. After the background plasma has forced the potential to drop below the gun energy (due to energy conservation, as discussed above), the number

of unneutralized electrons is instead determined by a balance between the injected current and cusp losses. Thereafter, the hot electron density depends on the background plasma density, only to the extent that the background might change the hot electron energy somewhat, and therefore its cusp loss rate. The fact that the number of hot electrons does not change much with background plasma density, while the potential changes a lot, creates an apparent problem with Poisson's equation, since $\nabla^2\phi$ is proportional to the unneutralized density. The resolution to this apparent conundrum is that as the density increases, the potential will be confined to an increasingly small sheath near the periphery, with the same excess charge producing a smaller potential.

The data shown in Figure 10a and 10b confirms this trend. The lower-density run, Figure 10a, has a potential that increases fairly smoothly with radius. The higher-density run, Figure 10b, has a potential that is quite flat until the sharp rise at about 65 cm. This trend is expected from the model.

5. Energy distributions

The model proposed in Section IV.B.2 predicts that the background plasma will force a decrease in the potential to a value below the gun energy, and that the energy of the background will be comparable to this potential. The hot electron population will maintain an energy somewhat less than its injection energy, because of energy conservation. Figure 11 clearly shows this trend, starting at times well below a ms, but becoming most apparent at the times that correspond to the rise in the background plasma density, a few ms.

V. Discussion

After extensive comparison of experimental results and theoretical analysis, we have developed a detailed description of the interaction between a hot electron gas and a plasma or vacuum background; this description has led us to an understanding of the properties of the electrostatic potential that is formed and maintained by the hot electron gas. We find that a model that describes the observations must include ionization of the background neutral gas, energy transfer between the hot electrons and cold plasma via the electrostatic potential, and wall recycling from bombardment by plasma lost through the magnetic cusps.

This model is detailed in the text of this paper, but in summary describes the experiment as follows.

(i) Electrons are injected at high energy and promptly (<1 μs) form a potential well comparable to their energy, $e\phi \sim E_{gun}$.

(ii) This well also accelerates any background plasma, which, by energy conservation, reduces the depth of the well, $e\phi \sim E_{gun} (n_{hot\ electron}/n_{background})^{\alpha}$, where α is a constant somewhat smaller than 1.

(iii) This inverse relation between $e\phi$ and $n_{background}$ continues to hold as n_b increases; n_b increases with time because of ionization of the initial neutral background gas by impact with hot electrons and the RF fields they produce, and because of ionization of an increasingly dense neutral background gas, which comes from the walls of the device due to bombardment of the wall by plasma escaping through the throats of the magnetic cusps.

This model explains why the potential shows an immediate decrease from $e\phi = E_g$ to $e\phi \leq E_g$ (the initial or promptly formed not very dense plasma shares energy with the injected electrons), why $e\phi$ then monotonically decreases with time (plasma density buildup from ionizing the background) and why at later time $e\phi$ decreases sharply to almost zero (very dense background plasma, because wall material has reached the center and been ionized). It also explains why higher current soon led to lower potentials (the higher current produced a higher background plasma density) and why higher energy e-guns, while initially giving higher $e\phi$, later gave lower $e\phi$ (the higher-energy gun had a correspondingly higher current, which gave a faster buildup of background plasma density, leading to lower $e\phi$).

One important result of this analysis is that the decrease of the plasma potential with time does not arise from some magical theorem that "nature abhors a non-neutral system," but rather plasma buildup from direct interaction with the wall. The cure follows from the analyses: wall conditioning must clearly be an important component of future experimental planning, particularly if long time operation is a consideration, where it will be necessary to bum out the neutral background, removing this energy sink from the device.

Future experiments on the Polywell fusion scheme should insist on higher-current sources for energetic electrons, and on isolating the wall from the plasma. Nevertheless, it is encouraging that the production and maintenance of a potential well in the present system showed that classical processes guide the characteristics of the system in the parameter ranges we have been able to explore, and that potential well formation and maintenance is not likely to be an anomalous element of this fusion approach.

Acknowledgments

We gratefully acknowledge the constant support and encouragement of Ira B. Kuhn, President of Directed Technologies, Inc. Without the vision of Robert Williams (DARPA), none of this work would have been possible.

The bulk of this study was funded by the Defense Advanced Research Projects Agency (DARPA), Contract No. MDA972-90-C-0006. The analysis in Section IV and the Appendix was supported in part under contract to Energy/Matter Conversion Corp., and in part by the Applied Plasma Physics Division of the Department of Energy Office of Fusion Energy.

Appendix: Formation and Confinement of a Background Plasma from a Prefill Gas Puff

The model presented in Section IV.B for the creation and time history of the potential produced by injecting electrons into a background gas included cold electrons, hot electrons, prefill gas, and interaction with the wall of the experimental chamber. To help validate some elements of this model, especially the elements involving the wall and the loss rate of the cold plasma, we performed a detailed study of the background plasma resulting from a gas puff ionized by the RF wave source described in Section III.

1. Experimental results

When the HEPS device is prefilled with a gas puff, the RF is turned on, and the plasma density is measured as a function of time, the results follow a very distinct and reproducible pattern, as shown in Figures 15-17.

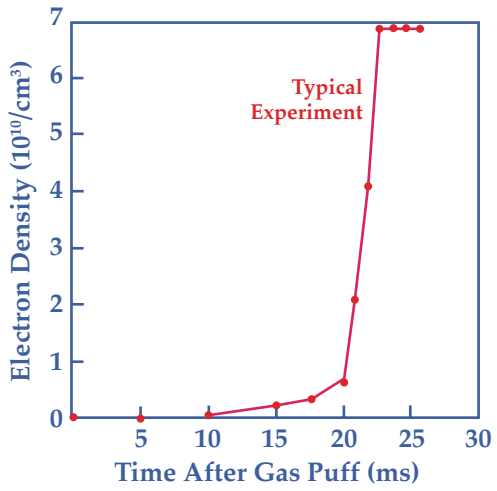

Figure 15 — Typical experimental result for electron density versus time with RF ionization of a prefill background, and no hot electrons.

The general behavior is that the plasma density, as measured by microwave interferometry, is observed to increase sharply with time to a peak density of order 7 x 10^{10} cm^{-3}, as shown in Figure 15. Some features of this behavior are as follows.

(i) The peak plasma density is only weakly dependent on the neutral prefill density.

(ii) The time at which the peak plasma density is reached is a very strong function of the neutral prefill density, as shown in Figure 16.

(iii) After the microwaves are turned off, the plasma decays with a profile $n_e(t)$ that is not exponential, $n_e(t) \neq n_e(0)e^{-t/\tau_{loss}}$, as shown in Figure 17.

(iv) The rise of density with time takes place on a time scale τ_R that is much shorter than the delay time τ_D at which the density rise is observed, implying that this is not exponential growth from a pre-fill breakdown, $n \neq n_p(0)e^{t/\tau_{breakdown}}$.

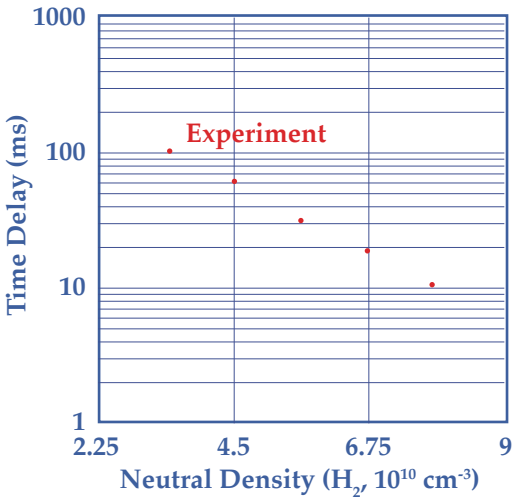

Figure 16 — Time delay for the density rise shown in Figure 19 versus fill density

2. Model

Consider a system in which a cold, neutral gas fills a chamber with density n_{o}, with a cusp magnetic field penetrating the chamber. We imagine the system to be controlled by the following behavior.

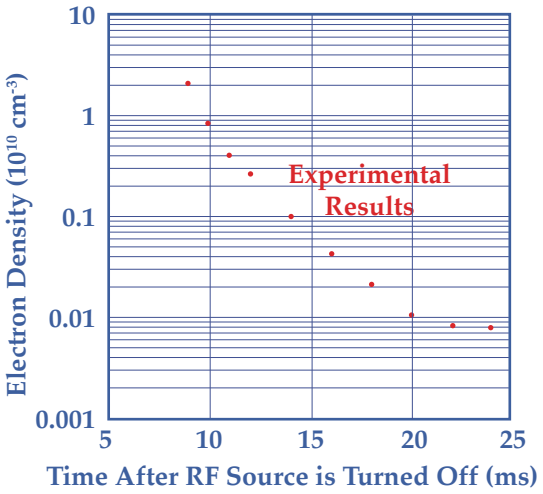

Figure 17 — Decay of electron density after the RF is turned off

(i) RF fields accelerate the free electrons in the system to some mean energy E_{o}, greater than the neutral gas temperature.

(ii) Some of these electrons are lost through the cusp field, at a rate τ_{e} of order 10^{-3} s.

(iii) Some of these electrons collide with, and ionize, the background gas.

(iv) Electrons that leave the system are relatively localized at the cusp holes, where they strike the wall of the chamber, producing wall neutrals that fill the system. The time scale for a cold neutral to cross the chamber is short, $<0.1 \times 10^{-3}$ s, for 1 eV neutrals.

(v) There is a finite amount of relatively weakly bound surface wall material at the electron loss sites, which is eventually exhausted by plasma bombardment of the wall.

(vi) After the surface material is cleaned off, a slower steady flux of wall neutrals is produced by plasma bombardment of the wall.

(vii) When the loose wall debris is exhausted, an increasingly large fraction of the neutrals in the chamber become ionized, so that the neutral density decreases until electron production no longer exceeds electron loss, and the growth of plasma density stops.

(viii) The electron density may then change only slowly, if the slow rate of neutral influx balances the rate of electron loss.

(ix) When the RF is turned off, warm electrons continue to ionize the (constant density) neutral background, but the electrons they produce stay cold, and do not avalanche.

(x) Thereafter, plasma density decays at a rate that changes in time as the energy of the trapped plasma decreases, with the fast electrons being lost first, followed by the cold electrons, which cool to a fraction of an eV due to the energy-selective loss process.

This description can be quantified, writing:

$$\frac{dn_p}{dt} = -\frac{n_p}{\tau} + n_p n_0 \sigma v \qquad \text{(A1)}$$

$$\frac{dn_0}{dt} = -n_p n_0 \sigma v + \left.\frac{dn_0}{dt}\right|_{wall\,material} \qquad \text{(A2)}$$

$$n_{0,\,wall\ material} = \frac{(4n_p t/\tau) n_{wall,\,\max}}{n_{wall,\,\max} + 4n_p t/\tau} + \frac{n_p t}{\tau} \qquad \text{(A3)}$$

Equation A1 describes the formation of plasma by collisional ionization of the neutrals, $n_p n_o \sigma v$, and the loss of the plasma at a rate $1/\tau$ determined from cusp confinement theory.[10] Equation A2 describes the depletion of neutrals due to ionization, where at $t = 0$, $n_o = n_{fill}$ as well as an increase in neutral density due to neutrals streaming in from the wall of the chamber. Equation A3 describes the production of neutrals by collision of warm plasma with the wall, first rapidly, until the bulk of the loose wall debris, $\simeq R^3 n_{wall\,max}$ has been knocked off by plasma bombardment, and then more slowly, giving steady-state production. Equation A3 assumes that one electron striking the wall produces five neutrals until the surface has been "cleaned" by the bombardment, after which one electron produces one neutral. The five-to-one ratio at early time is not essential to the analysis (three- or four-to-one would have been just as good). However, the one-to-one ratio at later time is required to explain the steady-state density observed at late time!

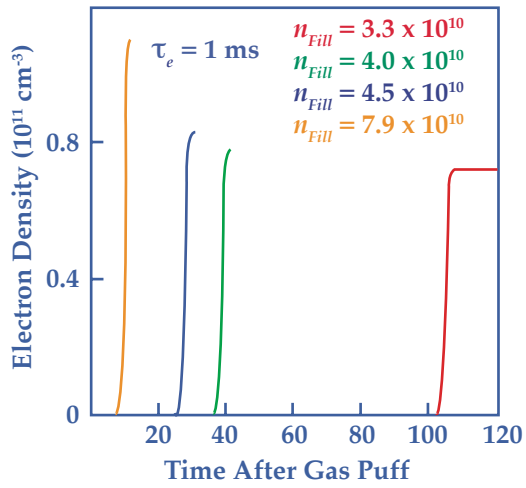

Figure 18 — Theoretical results for $n_e(t)$, varying n_{fill}

We solve Equations A1-A3 numerically, using the model described. We take τ = 1 ms, σv = 3.3 x 10^{-8} cm^3 s^{-1}, and $n_{wall,max} \simeq$ 7 x 10^{10} cm^{-3}. The value of $n_{wall,max}$ is the primary free parameter in the problem; σv and τ are reasonable order of magnitude estimates (actually $\sigma v\tau$ and n_M are the dominant parameters). Taking arbitrarily an electron density at t=0 of 10^3 cm^{-3}, and a prefill density varying between 3.3-7.9 x 10^{10} cm^{-3}, we obtain the results shown in Figure 18 for the density rise as a function of time. Varying n_{fill} gives a time of density rise shown by the line in Figure 19, labeled τ_e =1 ms.

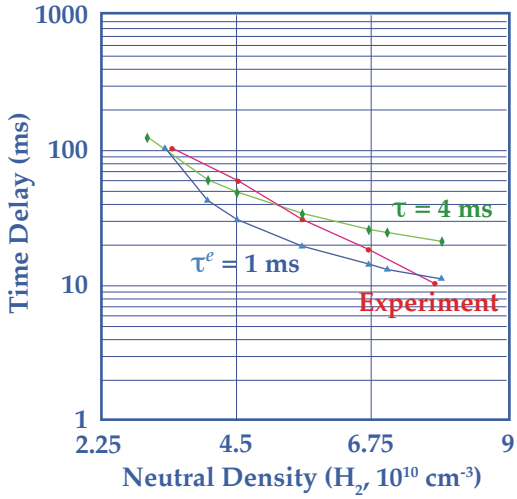

Figure 19 — Theoretical results for the time delay, with two electron confinement models. The experimental results are shown for comparison.

When the RF is turned off, the electron population has two components. First, there is a warm component, left over from the RF phase. It decays according to A1, but with σ=0, since now that the RF is turned off, collisions that ionize the background no longer produce warm electrons (when the RF was on, ionization produced warm electrons in a two-step process: the ionization itself produced cool electrons, but the RF ramped them up to a warm equilibrium temperature). The second component of the electron population consists of cold electrons produced when the warm electrons ionize the background; these cold electrons are lost by the usual escape mechanisms, i.e.,

$$\frac{dn_c}{dt} = -\frac{n_c}{\tau_c(t)} + n_p \sigma v n_0 \qquad \text{(A4)}$$

The loss rate τ_c increases with time because the energy decreases with time, both because there is less energy exchange with the warm component as $n_p \rightarrow 0$ and because cusp loss loses energetic particles faster than slow ones. Theoretically, the cusp loss time τ_c varies as $1/E^{\alpha}$, where $\alpha \leq 1$. We have taken τ_c (t=0) = 1.4 ms, somewhat larger than the decay time of the warm component, increasing to ~4 x (1.4) ms as $n_c >> n_p$. This gives the results shown in Figure 20.

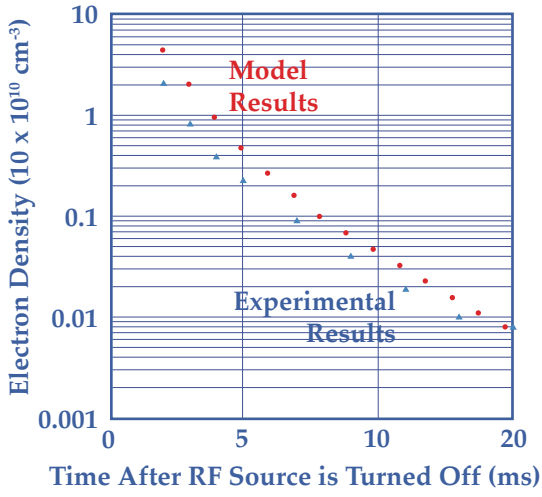

Figure 20 — Theoretical results for electron decay after RF shutoff. This compares well with experiment

To test the uniqueness of the model, we changed some of the assumptions on which it is based. First, we assumed that there is no wall material. The results are shown in Table 3. The result without wall neutrals shows a strong variation of n_{max} with n_{fill} in contrast with both the theory and the experiment, with the time behavior not much changed. If we assume that the fill density is depleted somewhat more slowly than $nn_o\sigma v$ due to continued influx of residual neutral fill gas, similar results are obtained, with n_{max} strongly dependent on $n_{fill}(0)$. If we remove the wall saturation effect, setting $n_{fwall,max} \rightarrow \infty$, the electron density either increases or decreases monotonically with time, depending on whether or not $dn_{o,wall}/dt > n_e/\tau_e$. If $dn_{o,wall}/dt = n_e/\tau_e$, a steady state is reached, with results shown in the last columns of Table 3. Again, the time behavior is not drastically changed, but the various plasma density reached is a strong function of n_{fill}.

Table 3 — $n_{e,max}$ and (delay time) versus n_{fill} for variations on the theory

n_{fill} cm^{-3}	Theory n_e, cm^{-3} (τ,ms)	No Wall n_e, cm^{-3} (τ,ms)	No max wall n_e, cm^{-3} (τ,ms)
3.3 x 10^{10}	7.2 x 10^{10} (106)	1.4 x 10^{8} (120)	3 x 10^{9} (200)
4.0 x 10^{10}	7.8 x 10^{10} (41)	1.4 x 10^{9} (50)	—
4.5 x 10^{10}	8.3 x 10^{10} (30)	2.8 x 10^{9} (34)	1.4 x 10^{10} (40)
5.6 x 10^{10}	9.3 x 10^{10} (19)	7.2 x 10^{9} (21)	2.6 x 10^{10} (24)
6.7 x 10^{10}	10 x 10^{10} (13.7)	1.3 x 10^{10} (15)	3.6 x 10^{10} (18)
7.0 x 10^{10}	11 x 10^{10} (12.7)	1.4 x 10^{10} (14)	—
7.9 x 10^{10}	11 x 10^{10} (10.8)	2 x 10^{10} (11.8)	4.8 x 10^{10} (14)

In order to make $dn_e/dt \simeq 0$ after reaching n_{max}, we took $dn_{e,wall}/dt = n_p/\tau$ at late time. If this condition is relaxed, the electron density behavior is much as before, except that after reaching a peak, the plasma decays, as shown in Figure 21. This emphasizes that the wall model is the essential feature in reproducing the experimental results.

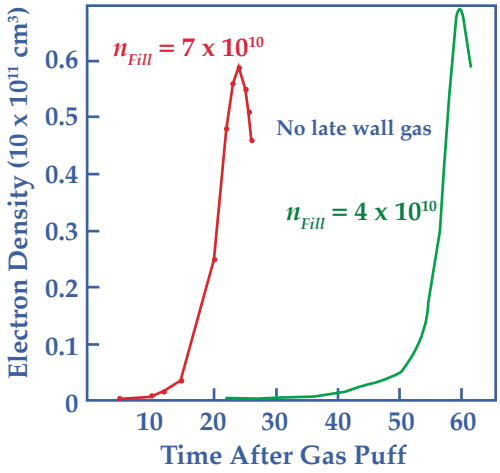

Figure 21 — Theory of $n_e(t)$ when the late influx of wall gas is omitted from the model

We conclude that the general behavior found in the HEPS experimental data for the density and time history of plasma produced by RF breakdown of a prefill gas can be explained by a model which includes cusp confinement of electrons and an influx of wall material produced by plasma bombardment, assuming an initially dirty wall. We have found no other model that adequately describes the experiment.

Publication History

Received April 18, 1994. Accepted October 6, 1994. Printed in January 1995, Physics Plasmas 2 (1).

Reformatted and color illustrations added August 2007 by Mark Duncan. Minor equation updating December 2008 and reference updating in April 2009.

References

[1] Robert L. Hirsch; Journal of Applied Physics, 38, 4522 (1967).

[2] Wilson C. Elmore, James L. Tuck. and Kenneth M. Watson; Physics Fluids 2, 239 (1959).

[3] Robert W. Bussard; "Method and apparatus for controlling charged particles," U.S. Patent 4,826,626, May 2, 1989.

[4] Robert W. Bussard; Fusion Technology, Volume 19, 273 (1991).

[5] Nicholas A. Krall; Fusion Technology, Volume 22, 42 (1992).

[6] R. Kelier and I.R. Jones; Z. Naturforschung. 21, 1805 (1966).

[7] John J. Watrous (private communication, 1990). Considerable research on this experiment was done in the period 1990-1993, in addition to that described in detail in the present paper. This included the gun injection simulations cited in the text.

[8] E.Y. Wang, Noah Hershkowitz, D. Diebold, T. Intrator, R. Majeski. H. Persing. G. Severn, B. Nelson, and Y. J. Wen; Journal Applied Physics, Volume 61, 4786 (1987).

[9] Theodore G. Northrop; *The Adiabatic Motion of Charged Particles*, Interscience, New York, 1963.

[10] J. Berkowitz, K.O. Friedrichs, H. Goertzel. H. Grad, J. Kileen. and E. Rubin; *Proceedings of the 2nd International Conference on Peaceful Use of Atomic Energy*, Geneva, 1958; (United Nations, Geneva. 1958), p. 177.